Supporting Information

White Light Emission from Lead-Free Mixed-Cation Doped Cs_2SnCl_6 Nanocrystals

Samrat Das Adhikari,[1*] Carlos Echeverría-Arrondo,[1] Rafael S. Sánchez,[1] Vladimir S. Chirvony,[2] Juan P. Martínez-Pastor,[2] Saïd Agouram,[3,4] Vicente Muñoz-Sanjosé,[3,4] Iván Mora-Seró[1,4*]

[1]Institute of Advanced Materials (INAM), Universitat Jaume I. Av. de Vicent Sos Baynat, s/n 12006, Castelló de la Plana, Spain.

[2]Instituto de Ciencia de Materiales(ICMUV), Universitat de Valencia, 46980 Paterna, Spain

[3]Department of Applied Physics and Electromagnetism, University of Valencia, Valencia 46100, Spain

[4]Materials for Renewable Energy (MAER), Unitat Mixta d'Investigació UV-UJI, Valencia 46010, Spain

Supporting Figures:

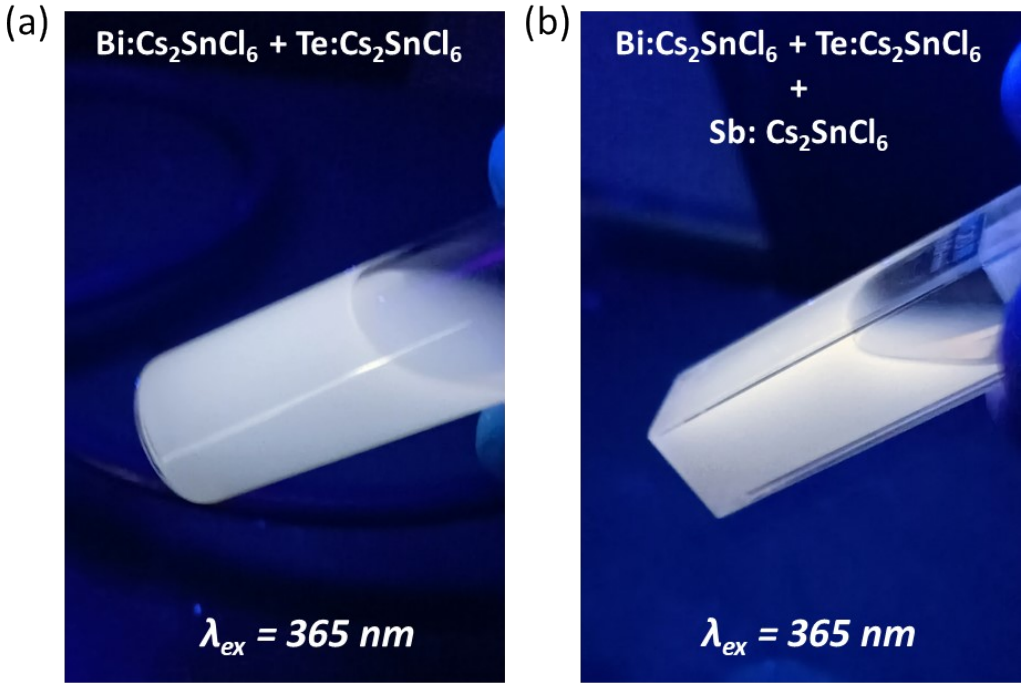

Figure S1. Digital images of suspensions obtained by post synthetic mixing of **(a)** blue and yellow emitting, and **(b)** blue, yellow and red emitting nanocrystals, both under illumination by a 365 nm UV lamp.

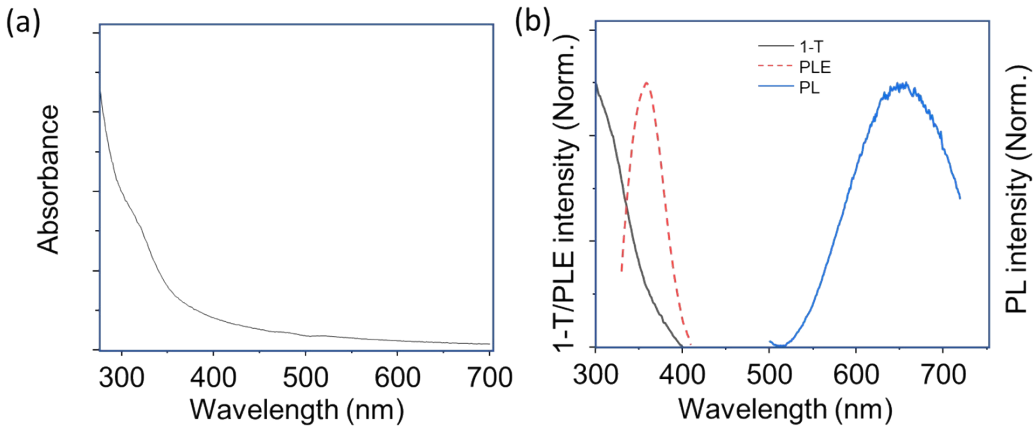

Figure S2. (a) UV-Vis absorbance and **(b)** PL, 1-T (where T is transmittance) and PLE spectra of Sb^{3+}-doped Cs_2SnCl_6 nanocrystals. The excitation and the emission wavelength for the measurements of PL and PLE were 350 nm, and 620 nm, respectively.

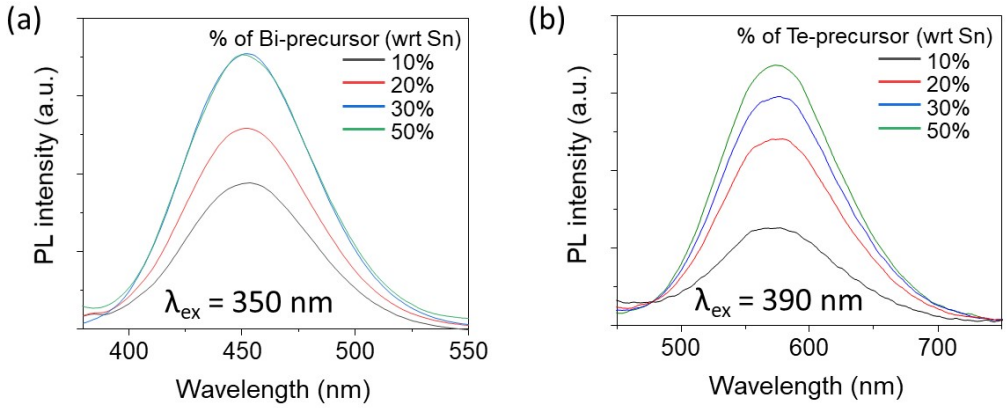

Figure S3. PL spectra of (a) Bi^{3+}-doped and (b) Te^{4+}-doped Cs_2SnCl_6 NCs at different precursor percentages with respect to the tin precursor. The excitation wavelength was 350 and 390 nm for Bi^{3+} and Te^{4+} doped Cs_2SnCl_6 NCs, respectively.

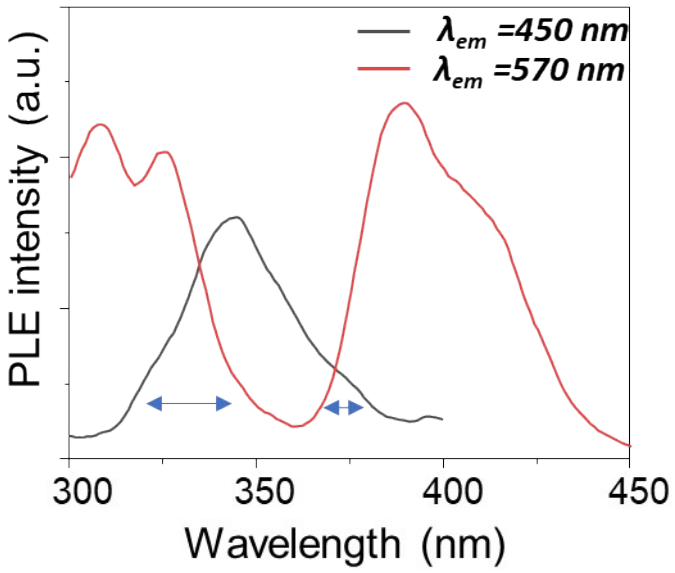

Figure S4. PLE spectra of Bi^{3+}/Te^{4+} dual-doped Cs_2SnCl_6 NCs obtained at emission wavelengths 450 nm, and 570 nm to show their common excitation spectral region.

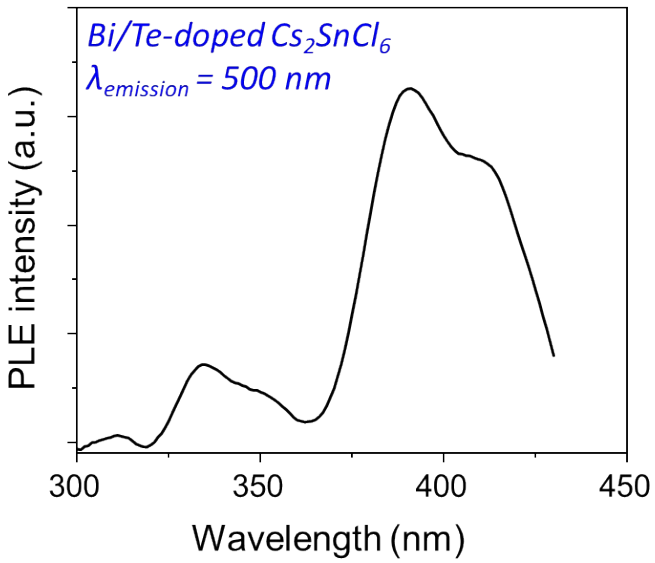

Figure S5. PLE spectrum of Bi^{3+}/Te^{4+} dual-doped Cs_2SnCl_6 NCs detected at 500 nm.

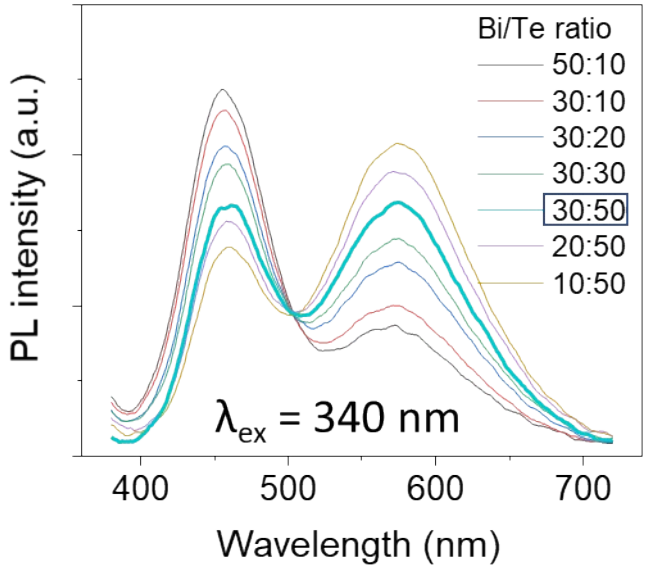

Figure S6. PL spectra of dual-doped (Bi^{3+} and Te^{4+}) Cs_2SnCl_6 with the variation of Bi and Te precursor ratio with respect to the tin precursor. The excitation wavelength for the PL measurements was 340 nm. The best obtained white emission (almost equal intensity of blue and yellow emission) was at 30:50 of Bi/Te precursor ratio (the bold spectrum).

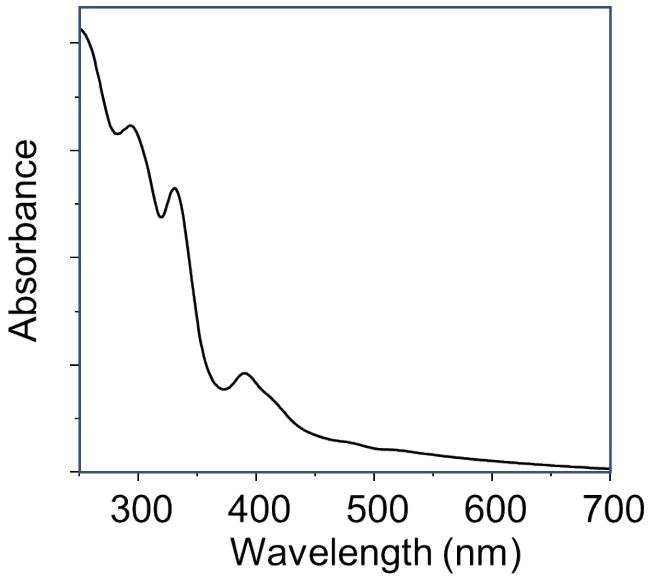

Figure S7. Absorbance spectrum of Bi^{3+}/Te^{4+} dual-doped Cs_2SnCl_6 NCs.

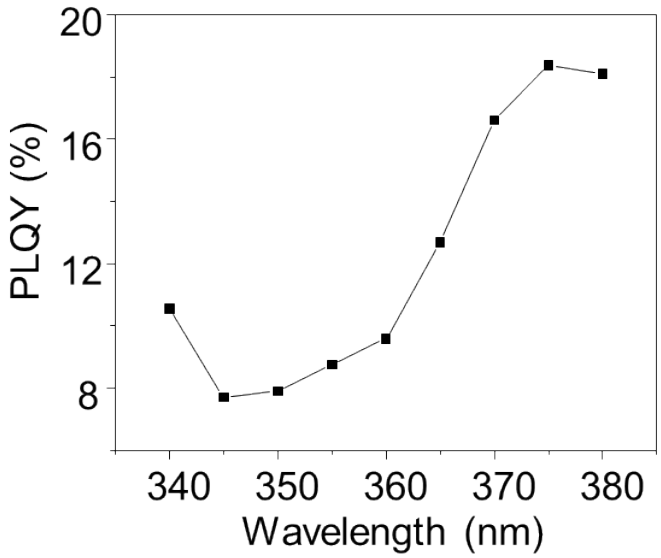

Figure S8. A plot of PLQY of Bi^{3+}/Te^{4+} dual-doped Cs_2SnCl_6 NCs dependence vs excitation wavelength.

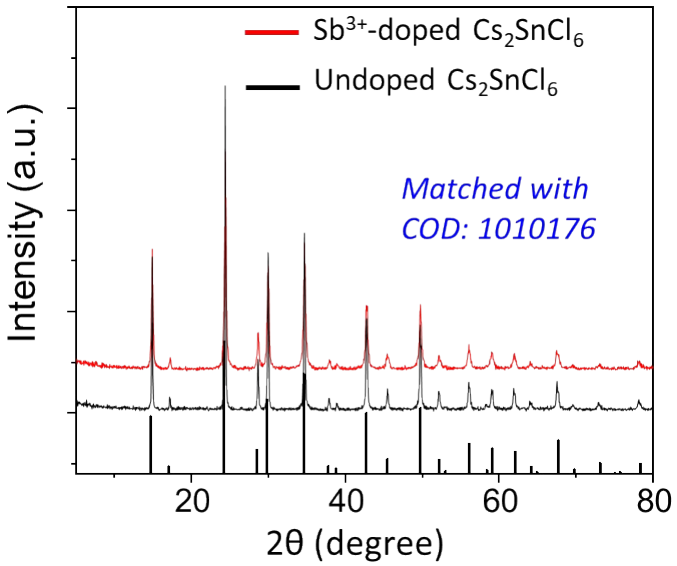

Figure S9. XRD patterns of Sb^{3+} doped Cs_2SnCl_6 and undoped Cs_2SnCl_6 NCs.

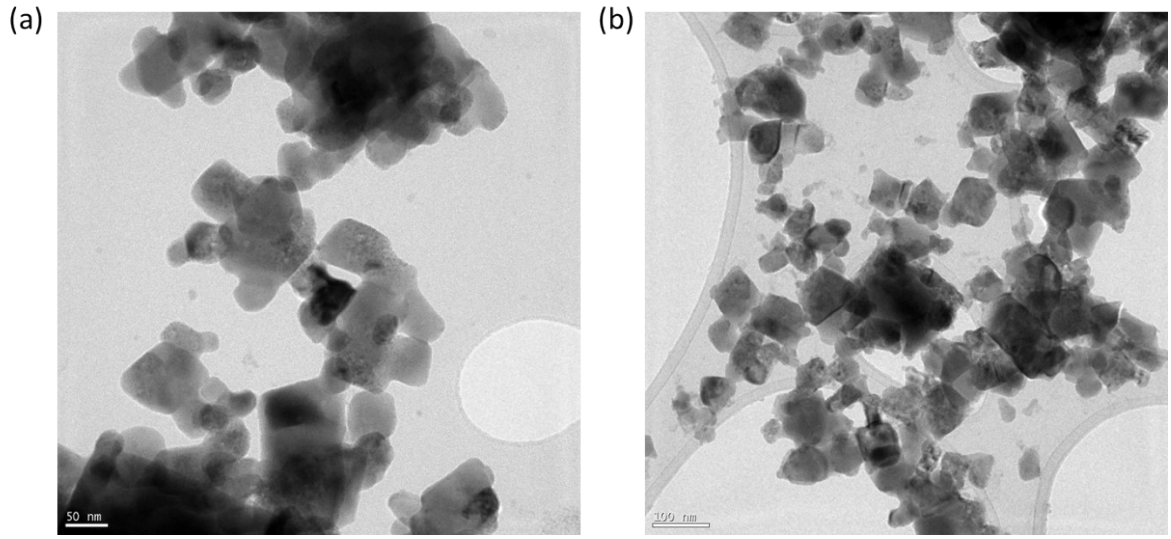

Figure S10. TEM images of (a) Sb^{3+} doped Cs_2SnCl_6 NCs and (b) undoped Cs_2SnCl_6 NCs.

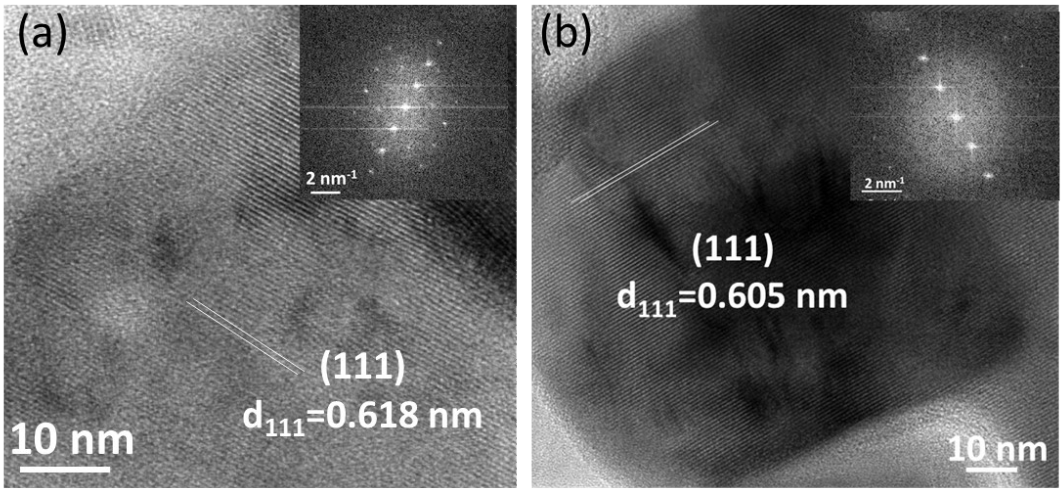

Figure S11. HRTEM images of (a) Sb^{3+} doped Cs_2SnCl_6 and (b) undoped Cs_2SnCl_6 NCs; inset shows corresponding FFT spots of (111) plane obtained from the HRTEM analysis.

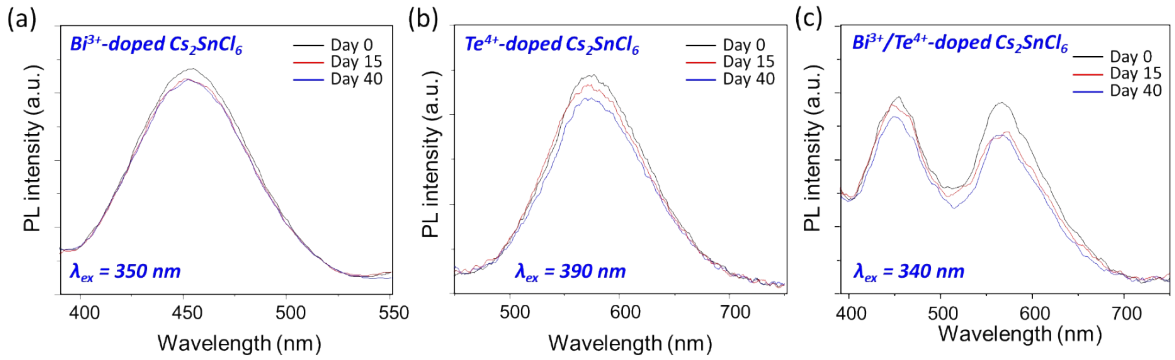

Figure S12. PL spectra of (a) Bi^{3+} doped Cs_2SnCl_6, (b) Te^{4+} doped Cs_2SnCl_6, and (c) Bi^{3+}/Te^{4+} dual-doped Cs_2SnCl_6 NC films after different times after synthesis. The excitation wavelengths for (a), (b), and (c) are 350 nm, 390 nm, and 340 nm, respectively. Corresponding PLQY values are provided in Table S11.

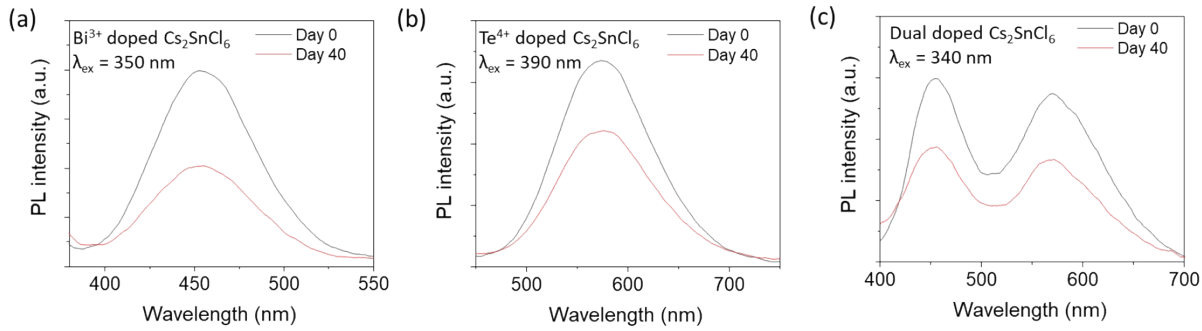

Figure S13. PL spectra of (a) Bi^{3+} doped Cs_2SnCl_6, (b) Te^{4+} doped Cs_2SnCl_6, and (c) Bi^{3+}/Te^{4+} dual-doped Cs_2SnCl_6 NCs after different times after synthesis. All the solutions were stored in an air-tight vial and kept under ambient condition. The excitation wavelengths for (a), (b), and (c) are 350 nm, 390 nm, and 340 nm, respectively. Corresponding PLQY values are provided in Table S12.

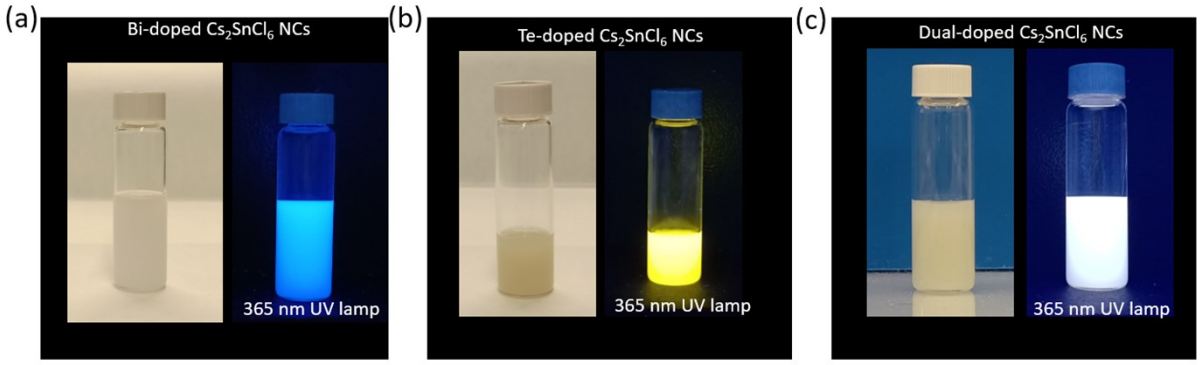

Figure S14. Digital images of stable dispersions of (a) Bi doped Cs_2SnCl_6, (b) Te doped Cs_2SnCl_6, and (c) Bi^{3+}/Te^{4+} dual-doped Cs_2SnCl_6 NCs in isopropanol obtained under ambient and 365 nm UV lamp illumination.

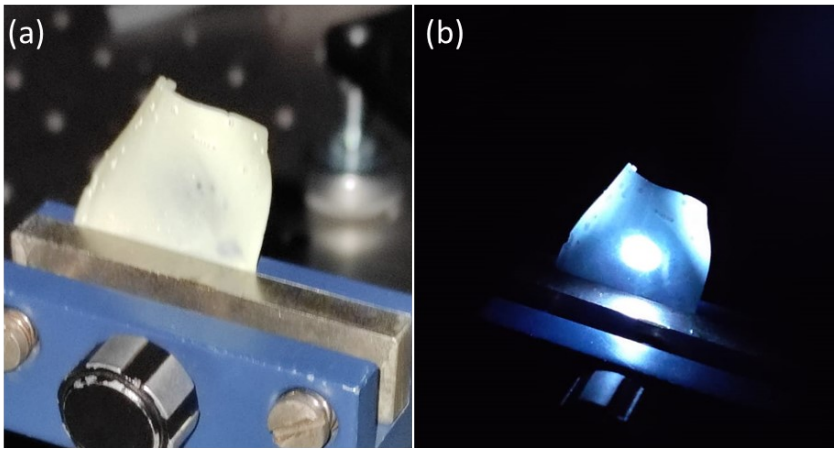

Figure S15. Digital images of the white light-emitting dual doped (Bi^{3+} and Te^{4+}) Cs_2SnCl_6 NCs embedded into a PMMA film under (a) ambient light and (b) under excitation with a 355 nm pulsed-laser; beam diameter ~1cm.

Supporting tables:

Table S1. PLQY of Bi^{3+} doped Cs_2SnCl_6 NCs at different dopant precursor intake with respect to the Sn-precursor, obtained from Figure S3a:

Dopant percentage (wrt Sn-precursor)	PLQY (%)
10	~10.6
20	~19.3
30	~26.5
50	~26.4

Table S2. PLQY of Te^{4+} doped Cs_2SnCl_6 NCs at different dopant precursor intake with respect to the Sn-precursor, obtained from Figure S3b:

Dopant percentage (wrt Sn-	PLQY (%)

precursor)	
10	~6
20	~21.6
30	~25.4
50	~28

Table S3. PLQY & CIE chromaticity coordinates (CIE-1931) of Bi^{3+}/Te^{4+} dual-doped Cs_2SnCl_6 NCs at different Bi & Te precursor ratio, obtained from Figure S6, at the excitation wavelength of 340 nm:

Dopant precursor ratio (Bi/Te)	PLQY (%)	CIE coordinate (x, y)
50/10	~10.1	0.25, 0.23
30/10	~9.7	0.26, 0.25
30/20	~9.3	0.29, 0.29
30/30	~9.8	0.31, 0.31
30/50	**~10.6**	**0.32, 0.33**
20/50	~11.2	0.35, 0.36
10/50	~11.8	0.37, 0.38

Table S4. CIE chromaticity coordinates (CIE-1931) of Bi^{3+}/Te^{4+} dual-doped Cs_2SnCl_6 NCs under different excitation wavelengths:

Excitation wavelength (nm)	CIE coordinate (x, y)	Color temperature (K)
340	**0.32, 0.33**	**6113**
345	0.27, 0.26	14019
350	0.25, 0.23	33430

355	0.23, 0.22	69604
360	0.25, 0.23	33430
365	0.25, 0.25	21065
370	**0.32, 0.32**	**6160**
375	0.37, 0.38	4309
380	0.39, 0.41	3976

The coordinates at 340 and 370 nm has the best match with the white-light emission coordinate.

Table S5. Elemental composition of Bi^{3+} doped Cs_2SnCl_6 NCs:

Elements	Atomic percentage
Cl	52.1
Sn	13.7
Cs	33.3
Bi	0.8

Table S6. Elemental Composition of Te^{4+} doped Cs_2SnCl_6 NCs:

Elements	Atomic percentage
Cl	48.3
Sn	14.8
Cs	34.2
Te	2.8

Table S7. Elemental Composition of Sb^{3+} doped Cs_2SnCl_6 NCs:

Elements	Atomic percentage
Cl	49.1
Sn	14.9
Cs	33.2
Sb	2.8

Table S8. Elemental Composition of Bi^{3+}/Te^{4+} dual-doped Cs_2SnCl_6 NCs:

Elements	Atomic percentage
Cl	50.6
Sn	12.8
Cs	32.8
Bi	0.6
Te	2.8

Table S9. Elemental Composition of undoped Cs_2SnCl_6 NCs:

Elements	Atomic percentage
Cl	47.6
Sn	18.3
Cs	34.0

Table S10. Tin precursor to dopant precursor intake ratios; and dopant ion percentage into final nanocrystals:

Material	Dopant precursor	Tin precursor to Dopant precursor ratios (in mmol)	Dopant percentage (%; in nanocrystals)
Bi^{3+} doped Cs_2SnCl_6	Bi(III) acetate	1:0.3	0.8-1
Te^{4+} doped Cs_2SnCl_6	Tellurium dioxide (TeO_2)	1:0.5	2.8
Sb^{3+} doped Cs_2SnCl_6	Sb(III) acetate	1:0.3	2.8
Bi^{3+}/Te^{4+} dual-doped Cs_2SnCl_6	Bi(III) acetate/TeO_2	1:0.3:0.5	0.6/2.8

Table S11. PLQY of the NC films were measured timewise.

Day(s) after the synthesis	PLQY (%)		
	Bi^{3+}-doped Cs_2SnCl_6 (ex 350 nm)	Te^{4+}-doped Cs_2SnCl_6 (ex 390 nm)	Bi^{3+}/Te^{4+} dual-doped Cs_2SnCl_6 (ex 340 nm)
0	~13.2	~15.2	~6.3
15	~12.9	~14.6	~5.3
40	~12.7	~13.1	~4.7

Table S12. PLQY of the NC suspensions (in acetone) were measured timewise.

Day(s) after the synthesis	PLQY (%)		
	Bi^{3+}-doped Cs_2SnCl_6 (ex 350 nm)	Te^{4+}-doped Cs_2SnCl_6 (ex 390 nm)	Bi^{3+}/Te^{4+} dual-doped Cs_2SnCl_6 (ex 340 nm)

0	~26.5	~28	~10.6
40	~10.5	~19.2	~7.9

Noteworthy, we obtained the reduced PLQY value while measured in films in comparison to the solution phase. However, these films were highly stable under ambient condition, only a negligible quenching of photoluminescence over time. In case of the solution, there is a noticeable quenching due to the evaporation of the harvesting solvent after long-time caused an ununiformed medium of the nanocrystals.

PLQY Calculations: The PLQY of dual-doped white-emitting Cs_2SnCl_6 nanocrystals have a higher intensity of emission at 340 nm than 370 nm (Figure 3b). Whereas, we obtained an opposite PLQY trend (Figure S3): 10.6 % under 340 nm excitation and 16.6 % under 370 nm excitation. This discrimination could be explained from the definition of PLQY, which is defined as the number of photons emitted divided by the number of photons absorbed. Herein, the material has a higher absorption at 340 nm than 370 nm. Hence, in spite of having the higher integral intensity of the emission at 340 nm than 370 nm, overall PLQY value experiences an enhancement at 370 nm.

Stokes shift calculations: The stokes shifts provided in Table 1 are calculated by subtracting PL maximum to the PLE maximum. Details of the calculations are provided below:

Bi^{3+}-doped Cs_2SnCl_6: (450-342) = 108 nm

Te^{4+}-doped Cs_2SnCl_6: (570-410) = 160 nm*

Sb^{3+}-doped Cs_2SnCl_6: (650-360) = 290 nm

*In case of Te^{4+}-doped Cs_2SnCl_6 NCs, there are two different absorption/PLE region: 300-340 nm, and 380-425 nm. The Stokes shift for this case has been considered from the lower energy peak maximum, i.e., 410 nm (peak-maximum of the shoulder peak from the higher wavelength absorption/PLE region).

Correlated color temperature (CCT) calculation: The CCT value was calculated following the McCamy's approximation[1]:

$CCT = 437n^3 + 3601n^2 + 6861n + 5517;$

$n = (x-0.3320)/(0.1858-y)$; where x, and y are the color coordinates.

Selection rule (Theory part): (i) The helicity of photons with either right-handed or left-handed circular polarization is +1 (σ^+) or -1 (σ^-), respectively, and linearly polarized photons are in a superposition of these two states. When a photon interacts with an electron in a crystal, it transfers its angular momentum and the resulting change in the magnetic total angular momentum quantum number m_j can be either +1 or -1 depending on the photon polarization. In accordance, an optical transition should fulfil that $\Delta m_j = \pm 1$, where m_j ranges from -j to j in unitary steps, $j = |l+m_s|$ is the total angular momentum quantum number, l is the orbital angular momentum quantum number, and m_s is the magnetic spin angular momentum quantum number.

(ii) According to the spin selection rule, the overall spin of a system must not change during an electronic transition, and arises from the Pauli exclusion principle, that states that wave functions for describing a many-electron system must be antisymmetric with respect to the exchange of any two electrons. This rule hence forbids that the promoted electron flips its spin.

(iii) In the case of materials with a centre of symmetry, octahedral complexes in particular, electronic transitions that conserve parity are forbidden. Since parity is defined as (-1), this rule forbids transitions between states with the same orbital angular momentum quantum number l, such as excitations between s- to s-like molecular orbitals, as well as p to p transitions. This selection rule, known as Laporte rule, applies to our Cs_2SnCl_6 compound, since it has octahedral symmetry around the Sn cation.

Possible optical transitions (Theory part): Provided that spin flip is forbidden, that is $\Delta m_s=0$, and that Δm_j should be either +1 or -1 to fulfil the conservation law of the angular momentum, the possible optical transitions for a spin-up electron are two: $|j, m_j\rangle = |^1/_2,^1/_2\rangle$ to $|^3/_2,^3/_2\rangle$, when it interacts with a photon of σ^+ polarization, and $|^1/_2,^1/_2\rangle$ to $|^3/_2,^{-1}/_2\rangle$ when the photon is σ^-; for a spin-down electron, the unique possible transition occurs between $|^1/_2,^{-1}/_2\rangle$ and $|^1/_2,^1/_2\rangle$ states (σ^+).

Reference

1. *C. S. McCamy, Color Res. Appl. 1992, 17, 142–144.*